POLITECNICO DI TORINO
Repository ISTITUZIONALE

Model calibration in the presence of resonant non-structural elements

Original
Model calibration in the presence of resonant non-structural elements / Matta, E., DE STEFANO, A.. - In: JOURNAL OF CIVIL STRUCTURAL HEALTH MONITORING. - ISSN 2190-5452. - 5:(2014), pp. 37-55. [10.1007/s13349-014-0096-1]

Availability:
This version is available at: 11583/2593160 since: 2020-04-29T12:57:37Z

Publisher:
Springer-Verlag

Published
DOI:10.1007/s13349-014-0096-1

Terms of use:

This article is made available under terms and conditions as specified in the corresponding bibliographic description in the repository

Publisher copyright
Springer postprint/Author's Accepted Manuscript

This version of the article has been accepted for publication, after peer review (when applicable) and is subject to Springer Nature's AM terms of use, but is not the Version of Record and does not reflect post-acceptance improvements, or any corrections. The Version of Record is available online at: http://dx.doi.org/10.1007/s13349-014-0096-1

(Article begins on next page)

26 November 2026

Manuscript
Click here to download Manuscript: Manuscript.doc
Click here to view linked References

Model calibration in the presence of resonant non-structural elements

Emiliano Matta*, Alessandro De Stefano

Department of Structural, Geotechnical and Building Engineering, Politecnico di Torino, 24 Corso Duca degli Abruzzi, Torino 10129, Italy

Abstract. Accurate finite element models are needed in many applications of Civil Engineering. Non-structural elements (NSEs) often interfere with the main structure, altering its stiffness and modal signature. Neglecting such interaction, although a common practice in design, may lead to unreliable predictions of the structural dynamic response and to biased interpretations of experimental vibrational tests. In the literature, the role of NSEs in vibration-based finite element model calibration is well documented for NSEs working "in parallel" with the main structure (e.g. masonry infills in buildings, pavements or railings in bridges) but remains essentially unexplored for NSEs working "in series" with the main structure (e.g. non-structural appendages like suspended ceilings, piping systems, storage tanks and antennas, but also partitions and façades in their out-of-plane modes). Through the analysis of numerical and experimental case studies, this paper shows that "in series" NSEs accidentally resonating with some structural mode may deeply contaminate the overall modal behaviour and severely invalidate model calibration, unless their role is properly addressed while performing experimental modal analysis and structural modelling. Two alternative calibration strategies are finally discussed which prove effective in the presence of resonant NSEs, based on respectively excluding/including the NSEs from/into the model structure.

Keywords: FE model calibration; experimental modal analysis; non-structural elements; resonant appendages; tuned vibration absorbers; modelling errors.

1. Introduction

Accurate finite element (FE) models are needed in many applications of Civil Engineering, ranging from health monitoring to structural control, from damage detection to structural evaluation and assessment [1]. Model accuracy can be conveniently improved by means of vibration-based FE model calibration, typically consisting in the reconciliation of the modal response of a baseline FE model with the experimental modal model derived from vibration data. Yet the success of model calibration is strictly conditional upon the adoption of a proper "model structure" for the baseline model, i.e. of an adequate form of the mathematical equations governing the problem and of the associated boundary conditions. Without choosing a proper model structure, or at least without recognizing the extent of errors in the adopted model structure, the analyst might reconcile to the measured data an incorrect or shifted model, which would eventually replicate measurements while lacking any sound physical meaning [2].

In Civil Engineering, a common source of modelling errors is represented by non-structural elements (NSEs), which may interact with the main structure (MS) altering its stiffness and modal signature. Neglecting such interaction, although a common practice in design, may lead to unreliable predictions of future dynamic scenarios and to biased interpretations of experimental vibrational tests. Simplifying, the interaction may essentially follow one of two alternative paradigms, which could be denoted for convenience as, respectively, P-NSEs and S-NSEs, according as they work "in parallel" (P-NSEs) or "in series" (S-NSEs) with the main structure. On the one hand, P-NSEs (e.g. masonry infills in buildings, pavements or railings in bridges and footbridges) enter the stiffness matrix of the FE model as a mere additive term, modifying frequencies and mode-shapes without affecting the model order. On the other hand, S-NSEs (e.g. non-structural appendages like suspended ceilings, piping systems, chimneys and parapets, storage tanks and antennas, electrical equipment and ornamentations, but also partitions and facades in their out-of-plane modes) introduce further degrees-of-freedom (DOFs) into the FE model, thus augmenting the modal model and potentially causing local/global modal interaction phenomena if accidentally "in resonance" with some structural mode, until eventually

* Research Scholar, Ph.D.; E-mail: emiliano.matta@polito.it; Phone: +39 011 090 4884; postal address: 24 Corso Duca degli Abruzzi, Torino 10129, Italy.

resulting into a deeply modified modal system. A schematic representation of the two types of NSEs on a single-DOF structure is proposed in Fig. 1.

In the current literature, the role of NSEs in vibration-based model calibration appears to be well documented for P-NSEs but essentially unexplored for S-NSEs.

In fact, P-NSEs are known to significantly influence both the static and the dynamic response of the main structure. Excluding P-NSEs from the model may result in:

- an underestimation of the vertical load bearing capacity of the MS, as in reinforced concrete bridges when barriers, sidewalks or diaphragms are excluded from the model [3], or in masonry bridges when fill material and pavement are neglected [4], or in metal roof deck diaphragms of building structures when non-structural roofing components are omitted [5];
- an underestimation of the horizontal load bearing capacity of the MS, or an inaccurate estimation of its expected response under code-conforming seismic [6] or wind [7] loads, as in moment resisting frame structures where masonry infills are excluded from the model;
- a bias in the outcome of vibration-based model calibration, as for a variety of non-structural and secondary structural elements in bridges (barriers, sidewalks and pavement [8], transverse bracings [9]), in footbridges (deck and handrails [10,11], asphalt pavement [12]), in buildings (cladding and internal partitions [13], stairs and elevators [14]), in wharves (non-structural steel frames and piping systems [15]), in stadia (precast seating deck units [16]).

On the other hand, several research works have dealt with the dynamic interaction between S-NSEs and the main structure, mostly to the purposes of predicting the seismic response of the combined system and providing simple design formulas to assess the seismic vulnerability of the non-structural components. Although non-structural appendages to buildings or industrial facilities are not part of the primary load-bearing structural system, their seismic analysis and design are in fact a topic of broad engineering interest [17,18]. Economic losses due to non-structural elements being damaged during past earthquakes have consistently been reported to be greater than those resulting from structural damage [19-21] and have urged most international building codes to account for this kind of failures [22]. The simplest and most popular approach to the analysis of S-NSEs is the so-called "cascade" approximation, in which feedback of the S-NSEs on the MS is neglected. In this approach, the MS and the S-NSEs are decoupled and analysed in sequence: at the first stage, the seismic response of the MS is evaluated neglecting the presence of the S-NSEs; at the second stage, the dynamic response of each S-NSE is evaluated considering the motion of the MS at the anchor points [23]. Following this approach, current building codes report closed-form expressions providing the seismic response of the S-NSE as a function of the floor structural response and the appendage-to-structure frequency ratio [24]. By neglecting the interaction between NSEs and the main structure, this "cascade" approximation may however lead to largely underestimate or overestimate the response of the secondary subsystem, especially if one or more of the natural frequencies of the NSE are tuned to those of the primary one [25]. Alternative to both the conventional "cascade" approximation and the rigorous but computationally expensive time-history analysis of the combined primary-secondary system under spectrum-compatible records, several approximate coupled solutions have been proposed in the literature [26]. These solutions generally consist in response spectrum analyses performed using the modal properties of the coupled system, obtained in approximate analytical terms from the modal properties of the uncoupled primary and secondary subsystems [27-29]. These studies are mainly intended to offer operative analysis tools for seismic design, but they also demonstrate the influence that resonant non-structural elements may have on the modal behaviour of the main structure. Similar approaches are used, in the same years, for dealing with resonant structural appendages of the "tuned mass damper" type, where the same interaction mechanism is exploited for the purposes of structural vibration absorption [30-33].

Despite such a conspicuous literature on S-NSEs, no proper attention seems to ever have been paid, to the best of the author's knowledge, to the influence that resonant S-NSEs may have on the accuracy of experimental modal analysis and vibration-based model calibration.

In this paper, numerical and experimental case studies are analysed in order to show the influence of resonant S-NSEs on the dynamics of the MS, and two alternative strategies are proposed to correctly perform model calibration in their presence. The material is presented as follows: in Section 2 the basic concept of local/global modal interaction is introduced for resonant S-NSEs, and the effects of neglecting such interaction at the modelling stage are exemplified through numerical simulations; in Section 3 numerical case studies are analysed to show that: (i) if modal interaction is not correctly identified during data interpretation, model calibration may result severely biased; (ii) if modal interaction is properly recognized, two successful approaches can be alternatively pursued, respectively based on excluding/including the S-NSEs from/into the model structure; in Section 4 the results from Section 3 are confirmed through a real case study, consisting in the experimental model calibration of a large-scale laboratory building structure where some S-NSEs are accidentally tuned to the main structure; in Section 5 conclusions are finally drawn.

2. Influence of non-structural elements on the modal response of the main structure

In this section, the two alternative paradigms of P-NSEs and S-NSEs are introduced. Their influence on the modal and time response of the main structure is numerically exemplified, assuming for the latter a planar, shear-type building schematization. Resonant S-NSEs, although not influencing the static response nor the horizontal load bearing capacity of the structure, are shown to deeply impact on the structural modal model and, in some cases, on the structural time response to design loads.

2.1 Basic configurations for P-NSEs and S-NSEs

A planar (2-dimensional) shear-type, N-storey building structure is assumed having, without loss of generality, $N = 3$ storeys and modal damping ratio $\zeta = 2\%$ in all the modes.

Four basic configurations will be compared herein, respectively denoted as:

- C_0, corresponding to the MS alone (Fig. 2a);
- C_1, corresponding to the MS having one or more P-NSEs (Fig. 2b);
- C_2, corresponding to the MS having one or more S-NSEs of the "single-anchor" type, such as pendulous appendages (Fig. 2c);
- C_3, corresponding to the MS having one or more S-NSEs of the "double-anchor" type, such as out-of-plane infills (Fig. 2d).

In order to better explain the peculiarities of the "in parallel" and "in series" arrangements, the mass and the stiffness matrices for the four configurations schematized in Fig. 2 are briefly derived as follows.

As far as configuration C_0 is concerned (Fig. 2a), the mass and stiffness matrices are as for classical shear-type frames:

$$\mathbf{M}_0 = diag\left(m_1, m_2, m_3\right) \tag{1.a}$$

$$\mathbf{K}_0 = \begin{bmatrix} k_1 + k_2 & -k_2 & 0 \\ -k_2 & k_2 + k_3 & -k_3 \\ 0 & -k_3 & k_3 \end{bmatrix} = ST\left(k_1, k_2, k_3\right) \tag{1.b}$$

where m_i is the mass at the i-th storey, k_i is the stiffness at the i-th inter-storey, *diag* denotes the diagonal matrix, and *ST* denotes the shear-type stiffness matrix operator, mapping the stiffness vector (k_1, k_2, k_3) into the stiffness matrix.

As far as configuration C_1 is considered (Fig. 2b), assuming for simplicity the mass m_p of the P-NSE be equally subdivided between the two adjacent storeys and denoting as k_p its stiffness, the mass and stiffness matrices are expressed by:

$$\mathbf{M}_1 = diag\left(m_1 + m_p/2, m_2 + m_p/2, m_3\right) = \mathbf{M}_0 + m_p diag\left(1/2, 1/2, 0\right) \tag{2.a}$$

$$\mathbf{K}_1 = ST\left(k_1, k_2 + k_p, k_3\right) = \mathbf{K}_0 + k_p ST\left(0, 1, 0\right) \tag{2.b}$$

The model order keeps the same as for C_0 (equal to N) and the stiffness matrix results from the summation of the stiffness matrix of the MS with the stiffness matrix of the P-NSE, as is typical of "in parallel" springs.

Considering the single-anchor appendage of configuration C_2 (Fig. 2c), on the other hand, a new DOF appears and the model order increases (up to N+1); assuming the appended mass to be concentrated in the new DOF and denoting as k_s the equivalent stiffness of the appendage, the mass and stiffness matrices become:

$$\mathbf{M}_2 = diag\left(m_1, m_2, m_3, m_s\right) \tag{3.a}$$

$$\mathbf{K}_2 = ST\left(k_1, k_2, k_3, 0\right) + k_s \begin{bmatrix} 0 & 0 & 0 & 0 \\ 0 & 1 & 0 & -1 \\ 0 & 0 & 0 & 0 \\ 0 & -1 & 0 & 1 \end{bmatrix} \tag{3.b}$$

In this case, as is typical of "in series" springs, the stiffness matrix results from the augmentation of the stiffness matrix of the MS (through the incorporation of one further row and one further column of null elements) and the subsequent addition of four more terms (plus or minus the stiffness of the S-NSE) at rows and columns corresponding to the DOFs of, respectively, the new appendage and the storey to which it is attached.

Finally, if the double-anchor appendage of configuration C_3 is considered (Fig. 2d), assuming for simplicity that half its mass be lumped at mid-span (where the new DOF is born) and that the remaining half be equally subdivided between the two adjacent storeys, and denoting as k_s its out-of-plane mid-span stiffness, the mass and the stiffness matrices can be expressed as follows:

$$\mathbf{M}_3 = diag\left(m_1 + m_s/4, m_2 + m_s/4, m_3, m_s/2\right) \tag{4.a}$$

$$\mathbf{K}_3 = ST\left(k_1, k_2, k_3, 0\right) + k_s \begin{bmatrix} 1/4 & 1/4 & 0 & -1/2 \\ 1/4 & 1/4 & 0 & -1/2 \\ 0 & 0 & 0 & 0 \\ -1/2 & -1/2 & 0 & 1 \end{bmatrix} \tag{4.b}$$

As for configuration C_2, also in this last case the stiffness matrix results from an augmentation and an addition (again an "in series" arrangement), although its structure becomes more complex since nine terms are added (instead of four) this time, at rows and columns corresponding to the DOFs of, respectively, the new appendage and the two anchor points.

2.2 Influence of NSEs on the modal response of the MS

In order to highlight the influence of NSEs on the modal response of the MS and particularly the effects of an erroneous modelling of NSEs, configurations C_1, C_2 and C_3 will be herein modelled either "correctly", i.e. according to Eqs. (1) to (4), or "incorrectly", i.e. according to the current practice of merely incorporating the mass of the NSEs into the structural mass while neglecting the contributions of NSEs to the structural stiffness. Thus, the incorrect modelling option will assume $\mathbf{K}_1 = \mathbf{K}_2 = \mathbf{K}_3 = \mathbf{K}_0$, $\mathbf{M}_1 = diag(m_1+m_p/2, m_2+m_p/2, m_3)$, $\mathbf{M}_2 = diag(m_1, m_2+m_s, m_3)$, and $\mathbf{M}_3 = diag(m_1+m_s/2, m_2+m_s/2, m_3)$.

Correct and incorrect modelling options are compared in Fig. 3, which shows both the correct (thick lines) and the incorrect (thin contours of grey areas) transfer functions from the ground acceleration to the maximum structural acceleration, for the following six different cases:

- Case (a): a single "in parallel" infill between the 1st and 2nd floors (as in configuration C_1), having mass equal to 5% of the total structural mass and stiffness equal to three times the inter-storey structural stiffness (i.e. $m_p/\Sigma m_i = 5\%$; $k_p = \Sigma k_i = 3k_i$).
- Case (b): a single "in series" pendulum anchored to the 2nd floor (as in configuration C_2), having mass equal to 2.5% of the total structural mass and frequency equal to the second structural frequency (i.e. $m_s/\Sigma m_i = 2.5\%$; $f_s = f_2$).
- Case (c): a single "in series" infill between the 1st and 2nd floors (as in configuration C_3), having mass equal to 5% of the total structural mass and frequency equal to the second structural frequency (i.e. $m_s/\Sigma m_i = 5\%$; $f_s = f_2$).
- Case (d): three identical "in parallel" infills, one at each inter-storey (in analogy with configuration C_1), having total mass equal to 5% of the total structural mass, and each one having stiffness equal to the inter-storey structural stiffness (i.e. $m_{pi}/m_i = 5\%$; $k_{pi} = k_i$).
- Case (e): three identical "in series" pendulums, one anchored to each floor (in analogy with configuration C_2), having total mass equal to 2.5% of the total structural mass, and having frequencies equal to, respectively, 0.95 (1st floor), 1.00 (2nd floor), and 1.05 (3rd floor) times the first structural frequency (i.e. $m_{si}/m_i = 2.5\%$; $f_{s1} = 0.95f_1$; $f_{s2} = 1.00f_1$; $f_{s3} = 1.05f_1$).
- Case (f): three identical "in series" infills, one at each inter-storey (in analogy with configuration C_3), having total mass equal to 5% of the total structural mass, and having frequencies equal to, respectively, 0.95 (1st floor), 1.00 (2nd floor), and 1.05 (3rd floor) times the first structural frequency (i.e. $m_{si}/m_i = 5\%$; $f_{s1} = 0.95f_1$; $f_{s2} = 1.00f_1$; $f_{s3} = 1.05f_1$).

Common to all six cases, the underlying main structure (configuration C_0, not described in Fig. 3) is assumed to have the same mass at every storey ($m_1 = m_2 = m_3$), the same stiffness at every inter-storey ($k_1 = k_2 = k_3$) and a fundamental frequency $f_1 = 1$ Hz, with its second and third frequencies being consequently equal to $f_2 = 2.8019$ Hz and $f_3 = 4.0489$ Hz. Common to all S-NSEs, a 2% damping-ratio is assumed in all simulations.

Fig. 3(a) and 3(d) show the obvious effect of P-NSEs being inserted into the MS, consisting in an increase of the natural frequencies, more or less generalized depending on the number and location of the P-NSEs. The dynamic behaviour proves deeply modified, yet the modal order keeps unaltered (three natural modes). This phenomenon is well-known and in most cases easily detectable during model calibration even if not specifically accounted for in the model, since resulting in updated MS stiffness values much larger than expected. And even if not explicitly recognized by the analyst, this interaction mechanism would be someway implicitly understood by the calibrated model itself, whose overall stiffness description would phenomenologically resemble the true one. Examples of NSEs obeying this paradigm of "in-parallel" interaction with the main structure include: cladding, internal partitions, stairs and elevators in buildings; pavements, railings, barriers, sidewalks in bridges; fill material in masonry bridges; deck and railings in footbridges; non-structural steel frames and piping systems in industrial facilities. The literature reports several real case studies where this "in-parallel" interaction plays a significant role in dynamic identification and model updating.

Fig. 3(b), 3(c), 3(e) and 3(f), on the other hand, show the effect of resonant S-NSEs being inserted into the MS. Such insertion generates new modes, one for each appendage, closed to (and interacting with) the original structural modes, resulting in the transfer functions being deeply modified in the vicinity of the NSEs' resonant frequencies while basically unaltered far from it. This phenomenon, easily explicable using the same theoretical framework developed to describe tuned vibration absorbers [30] yet so far undocumented for NSEs in model-updating applications to the best of the authors' knowledge, may significantly bias model calibration if not adequately recognized, as it will be demonstrated in the sequel. Examples of NSEs obeying this paradigm of "in-series" interaction with the main structure may include a variety of secondary structural and non-structural appendages in buildings or industrial facilities: piping systems, machinery, non-structural steel frames, storage tanks, chimneys and antennas, partitions and facades in their out-of-plane modes, parapets, suspended ceilings, ornamentations. If the natural frequencies of these S-NSEs are far from the structural modal frequencies, the dynamic interaction may be of scarce practical interest, and insignificant discrepancies are expected between the "correct" and "incorrect" modelling options. If instead the S-NSEs are close to resonance with some structural mode, and their mass is a non-negligible percentage (e.g., about 5% in the present numerical case studies) of the effective modal mass of the interacting structural mode [30], then the effects of the interaction grow important, and the correct and incorrect options lead to meaningful differences.

To better explain the modal consequences of an erroneous modelling of NSEs, Fig. 4 reports the natural frequencies and the mode-shapes for the same Cases (a) to (f).

Results obtained using the correct modelling option are plotted as grey-scale coloured marks (placed at the height of the model DOFs) connected by dotted lines; results obtained using the incorrect modelling option are plotted in continuous lines. Cases (a) and (d) confirm that the incorrect modelling of P-NSEs leads to erroneous frequencies and mode-shapes but not to an erroneous model order. If, as in Case (d), the additional stiffness matrix contributed by the P-NSEs is exactly proportional to the stiffness of the MS, then correct and incorrect mode-shapes result obviously equal, while correct and incorrect frequencies result proportional to each other. On the other hand, as far as S-NSEs are concerned, the incorrect modelling provides a 3-DOF FE model (with modes only slightly altered with respect to those of the MS due to the slight increase of the mass matrix coefficients), whilst the correct modelling increases the model order by the number of the appendages' DOFs, eventually leading to four modes in Cases (b) and (c) and to six modes in Cases (e) and (f). For the mere sake of convenience, the cluster of interacting modes born from the interference of the S-NSEs with a particular structural mode is here named after such structural mode, and in fact comprises modes 2a and 2b in Cases (b) and (c), and modes 1a, 1b, 1c and 1d in Cases (e) and (f). The new modes possess frequencies which are distributed around the original frequency of the MS and, remarkably, possess mode-shapes which are virtually indistinguishable from each other as well as from the original mode-shape of the bare MS, except at the DOFs corresponding to the NSEs, i.e. unless measurements are taken at the NSEs. Modes far from the NSEs' frequencies appear instead almost unaffected by their presence. Noticeably, these results have been obtained assuming relatively small appendage-to-structure mass ratios and non-unitary appendage-to-structure frequency ratios. Although not shown in the present paper, the damping ratio of the new, combined modes proves to be a weighted average of the damping ratios of, respectively, the S-NSE and the interacting structural mode, the weight depending on the ratio of the NSE mass to the modal mass of the structural mode and on the NSE position along the structure, in full agreement with the classical theory of tuned mass dampers [30, 31]. Because of the larger uncertainties inherent in experimental damping identification and of the relatively limited use of model updating for the specific purpose of modal damping calibration, the influence of S-NSEs on structural damping is not further emphasized in the present paper and is left for future work.

Two main conclusions can be drawn from this simple preliminary example, regarding the potential effects of errors inherent in, respectively, modelling and identification:

- first (and more intuitively), an incorrect modelling of S-NSEs may prevent a physically meaningful reconciliation of the FE model with a correctly identified modal model;

- second (and less obviously), an inaccurate experimental modal identification, perhaps biased by the expectation of an N-modes structure, may mislead the analyst to (randomly) reject all but one of the interacting modes within any frequency cluster, which can potentially result in even more severe consequences on the reliability of the calibration process, as will be better explained in the next pages.

2.3 **Influence of S-NSEs on the time response of the MS**

In order to highlight the influence of S-NSEs on the time response of the MS and particularly the effects of an erroneous modelling of S-NSEs, the shear-type building structure introduced above is simulated under the action of a set of 338 historical seismic records extracted from the PEER-NGA Strong Motion Database [34]. Various configurations of S-NSEs are considered, either correctly or incorrectly modelled, including Cases (e) and (f) defined above and a new Case (f*), obtained as a variant of Case (f) by assuming that the three identical "in series" infills have frequencies equal to r times the fundamental structural frequency f_1 and total mass equal to μ times the total structural mass.

In Fig. 5 the acceleration time-history at the 3rd storey is reported for two selected seismic records, in both cases of correct (black line) and incorrect (grey line) modelling of the S-NSEs. Fig. 5(a) describes Case (e) under Record # 0143 TAB-LN (Tabas earthquake, 09/16/78). Fig. 5(b) describes Case (f) under Record # 1529 TCU102-N (Chi-Chi earthquake, 09/20/99). Denoting as R the response ratio obtained dividing the correct by the incorrect maximum accelerations, Fig. 5(a) and 5(b) provide R = 1.562 and R = 0.523, respectively. It is evident that an incorrect modelling of S-NSEs may significantly affect not only the modal response but also the time response of the overall system.

In Fig. 6 the response ratio is plotted for the whole set of 338 records. Fig. 6(a) refers to Cases (e) and (f). Fig. 6(b-c) refer to Case (f*), assuming a mass ratio μ = 5% and seven different values of the frequency ratio r, respectively ≤ 1 (Fig. 6b) or ≥ 1 (Fig. 6c).

In Fig. 7 three selected percentiles, extracted from response ratio curves obtained for the 338 records as in Fig. 6, are plotted as a function of the frequency ratio r for three possible values of the mass ratio, namely μ = 2.5%, 5% and 10%. Similar results, not reported for the sake of brevity, were obtained changing the stiffness and the damping ratio of the MS.

Results in Fig. 5 to 7 demonstrate that incorrect modelling of S-NSEs may significantly bias the prediction of the maximum response to specific ground motions if the frequency of some S-NSE is close to the frequency of some structural mode, to an extent which gets larger as the mass of the S-NSE increases. Fortunately, the bias results statistically conservative, in that neglecting the dynamics of the appendages implies on average an overestimation of the response, as shown by the 5% percentiles deviating from unity more than the 95% percentiles, and by the mean being systematically less than or equal to unity, once again confirming the analogy existing between S-NSEs and passive tuned vibration absorbers.

In other words, neglecting resonant NSEs seems generally acceptable within the scope of seismic design and assessment of structures. Nevertheless, the structural response to single seismic records proves very sensitive to the presence of resonant NSEs, and this again shows the extent to which S-NSEs can modify the modal behaviour of the housing structure.

3. **Model calibration in the presence of resonant non-structural elements: a numerical case study**

In this section the effect of resonant S-NSEs on modal identification and model-updating is demonstrated by means of a simple numerical simulation performed on the structural system already encountered in Section 2 and there denoted as Case (c).

An incorrect baseline model is supposed to be initially available, characterized by a shear-type MS having three uncertain stiffness parameters, k_1, k_2 and k_3 (requiring calibration), and structural masses exactly known, and by masonry infills incorrectly modelled as assumed in Section 2, i.e. as merely a pair of rigid masses incorporated into the floors' masses.

Structural vibrations are supposed to be measured by accelerometers located exclusively at the three storey levels (i.e. with no accelerometer available on the NSE), and experimental modal identification is supposed to be performed in order to calibrate the baseline model.

Various scenarios may occur, mostly depending on: (i) the correctness of the performed modal identification, and (ii) the importance of achieving modelling accuracy. Three main approaches are conceivable, briefly sketched as follows.

3.1 **Approach 1 (incorrect identification plus incorrect model)**

According to Approach 1, the influence of the NSE is supposed not to be understood by the analyst who, expecting a 3-DOF system (according to the incorrect baseline model), looks for three structural modes only and, perhaps deceived by measurement noise, identifies them as, for instance, f_1, f_{2a} and f_3 (or, which would be the same, as f_1, f_{2b} and f_3). Using the incorrect 3-DOF model, the analyst will calibrate the three stiffness parameters, k_1, k_2, k_3, so that the analytical frequencies of the FE model would match the experimentally identified frequencies. In looking for modal reconciliation, the analyst might also use mode-shapes to build the error function but, regarding them as less accurate than frequencies and assuming the problem as exactly determinate (3 data and 3 unknowns), he will likely prefer to only rely on frequencies in this case. Anyway, Fig. 4 suggests that, because of the similarity between correct and incorrect mode-shapes (except at the unmeasured DOF of the NSE), using mode-shapes as further source of information would scarcely improve results.

3.2 **Approach 2 (correct identification plus incorrect model)**

According to Approach 2, the influence of the NSE is supposed to be understood by the analyst who, identifying four real modes and attributing modes 2a and 2b to the interaction between the S-NSE and the second structural mode, recognizes the 3-DOF model as inadequate to reproduce them all. However, being supposedly not interested in an accurate modelling of the NSE and of the second mode, he will consider it an unnecessary cost to modify the model structure so as to include the NSE, and will prefer to keep the baseline model structure unaltered (incorrect modelling).

Since the four identified modes are incompatible with the three simulated modes, the analyst will exclude modes 2a and 2b from the experimental data and will calibrate the model on the basis of the first and third modes only. Since, however, two frequencies are insufficient to calibrate three unknown stiffness parameters, the analyst will avoid the indeterminateness of the problem (i.e. non-uniqueness of the solution) by using mode-shapes too, for example mode-shapes 1 and 3. If no mode-shapes were available from the identification this approach would not be viable unless the analyst could reduce the number of unknowns by making some further *a priori* assumption. This approach seems of particular advantage when multiple S-NSEs are attached to the MS at different points and there is not enough information to identify the one(s) responsible for the tuning effect.

3.3 **Approach 3 (correct identification plus correct model)**

The influence of the NSE is understood by the analyst who, based on the correct identification of the four true modes, accepts to improve the model so as to account for the S-NSE. Still assuming the masses as completely known, he will update the four unknown stiffness parameters, k_1, k_2, k_3 and k_s, (see again Fig. 2(d)) using the four identified frequencies.

3.4 **Comparison of the three approaches**

The three approaches above are obviously only some of the possible options the analyst might follow to perform model calibration in the presence of S-NSEs. Alternatively, he might use redundant information to increase robustness. Or, once recognized the significance of the NSE (Approaches 2 and 3), he might decide to repeat acquisitions, processing and calibration after deploying additional sensors on the NSE. Anyway, in their simplicity, these three approaches have the merit, on the one hand, to indicate two viable strategies for dealing with S-NSEs in model calibration (Approaches 2 and 3) and, on the other hand, to underline the drawbacks of not following them (Approach 1).

Results are summarized in Table 1, with Approach 1 presented twice, according as either f_{2a} (Approach 1-a) or f_{2b} (Approach 1-b) be used for updating. Table 1 presents the optimal solutions of the calibration problem (herein obtained using a hybrid direct-search algorithm, consisting of a genetic algorithm followed by a nonlinear least-square solver), corresponding to finding the normalized updating parameters $\overline{k}_i$ (defined as the dimensional parameters divided by their nominal value) which numerically minimize the following objective function:

$$f_{ob} = \sqrt{\left(\sum_i (f_i / f_{ei} - 1)^2 + \lambda^2 \sum_j \left\| \varphi_j - \varphi_{ej} \right\|^2 \right) \Big/ \left(\sum_i (1) + \lambda^2 \sum_j (1) \right)} \qquad (5)$$

in which the first summation (subscript i) refers to the frequency residual and the second summation (subscript j) to the mode-shape residual ($\sum_i (1)$ and $\sum_j (1)$ in the denominators standing for the total number of, respectively, frequency and mode-shape residuals), f_i and f_{ei} being, respectively, the analytical and the experimental natural frequencies, ϕ_j and ϕ_{ej} being the analytical and the experimental mode-shapes (normalized

so as to have unit norm), $\|\varphi_j - \varphi_{ej}\|$ being the 2-norm (or Euclidean distance) between vectors ϕ_j and ϕ_{ej}, and λ being the relative weight assigned to the mode-shape residual with respect to the frequency residual, accounting for the different reliability of mode-shape information with respect to frequency information and herein taken to be equal to 1. It is worth noticing that the analyst might choose to include into Eq. (5) only a selected subset of the available frequencies (subscript *i*) and mode-shapes (subscript *j*), with the frequency subset and the mode-shapes subset not necessarily being the same; supposing that the two subsets be the same, Eq. (6) further simplifies as follows:

$$f_{ob} = \sqrt{\left(\sum_i [(f_i / f_{ei} - 1)^2 + \lambda^2 \|\varphi_i - \varphi_{ei}\|^2]\right) \Big/ \left(\sum_i (1+\lambda^2)\right)} \tag{6}$$

Eqs. (5) and (6) are so conceived that if all residuals equal a certain value then f_{ob} equals that same value. In this sense, f_{ob} is the weighted error of the analytical modal model with respect to the experimental modal model. Besides the updated parameters, Table 1 presents, in the last column, their RMS (root mean square) distance from their true value (1.000 in the present case), herein denoted as *d* and taken as a measure of the calibration error. The value of the objective function, f_{ob}, not reported in Table 1, is virtually null in this numerical example for all cases.

Based on Table 1 the following observations can be made:

- an incorrect modal identification (Approach 1) may lead to unacceptable errors in the parameter domain (*d* = 33.6%);
- understanding the true "modal structure" while keeping an incorrect FE "model structure" (Approach 2) may lead to acceptable calibration errors (2.7%);
- a correct identification combined with a correct NSEs' modelling (Approach 3) is obviously the best option, which in the present ideal case leads to a null error in the parameter domain as a consequence of the assumed absence of errors in the identified modal data as well as in the model structure.

The validity of these results will be tested on a real case study in the next section.

4. Model calibration in the presence of resonant non-structural elements: an experimental case study

The present section shows the influence of resonant NSEs on model calibration by means of an experimental case-study.

4.1 The test structure

The test structure is a large-scale (2:3) model of a two-storey steel frame building with composite steel-concrete floors (Fig. 8(a)). Built at the Structural Laboratory of the University of Basilicata (Italy), it served as a benchmark for the experimental assessment of the seismic effectiveness of different passive and semi-active control strategies, in the framework of the inter-university Italian DPC-ReLUIS 2005-08 Project.

The steel structure, consisting of columns and beams orthogonally interconnected into a regular (doubly-symmetrical) three-dimensional frame with one bay in both directions and two rectangular floors (levels 1 and 2), is mounted on a rigid horizontal base (level 0), resting on two sliding guides and connected to a dynamic hydraulic actuator which can impart the desired mono-dimensional excitation to the structure. Four HE140B columns, fixed to the base, extend continuously to the top floor. Eight IPE180 lateral beams, welded to the columns, support the two composite floors, made up of concrete slabs cast on coffer profiled steel sheeting. Columns' free length is 4.00 m, divided into two 2.00 m inter-storey heights. Beams' length is 4.00 m in the along-excitation (longitudinal or *x*) direction and 3.00 m in the across-excitation (transverse or *y*) direction. Floors' thickness is larger than expected and non-uniform because of a sagging effect occurred during concrete casting. In order to house the dissipating devices during tests on the controlled structure, four HE100A V-inverted braces, crowned with gusset plates, are bolted at both storeys, parallel to the longitudinal direction.

At the initial stage of the Project, the need of an accurate, experimentally calibrated FE model of the benchmark building motivated a preliminary campaign of dynamic tests which was conducted on the structure in its original, uncontrolled configuration, i.e. with no dissipative devices installed between the top of the V-inverted braces and the beams. In this configuration, the V-inverted braces clearly behave like secondary appendages connected at their base to the supporting beams and free at their top, and can be then classified as non-structural elements of the "in series" type (the two upper braces working "in series" with the first storey level, the two lower braces working "in series" with the base level), very stiff in the their in-plane direction (*x* axis) and relatively flexible in their out-of-plane direction (*y* axis). The significance of braces' dynamics was

however not immediately understood and, as it will be clarified in the sequel, their influence on the overall structural behaviour was initially neglected on the account of their relatively small mass, with the result that the original baseline FE model reported no trace of their presence.

In order to increase the amount of experimental data available, classical "perturbed boundary condition testing" was applied [35], consisting in perturbing both the structure and the analytical model by adding the same amount of mass at given positions. A total of eight concrete blocks (about 340 kg each) were fixed onto the floors during testing according to three different configurations. Starting from the basic configuration (BC), characterized by no additional mass, a second doubly-symmetric configuration (SC) was obtained by the addition of four blocks on each storey, and finally a non-symmetric configuration (NC) was obtained by removing two blocks from the SC configuration at each storey.

For each of the three mass configurations, ambient vibration tests were conducted on the uncontrolled structure, keeping the sliding guides locked. The dynamic response was measured, at a sampling frequency of 200 Hz, by 15 uniaxial high-sensitivity force balance Columbia SA107LN accelerometers (operating in the range ±0.1 g). The location of the accelerometers and of the concrete blocks is described in Fig. 8(b). Significantly, no sensors were placed on the upper braces.

4.2 **The initial FE model (excluding NSEs)**

The FE model available at the initial stage of the project was, as anticipated above, the model of the MS alone, with no consideration for the dynamics of the NSEs, their mass being merely included into the mass of the floor slabs. This was partly because the mass of the appendages was seen to be small with respect to the structural mass, partly because there was no interest to accurately simulate braces' out-of-plane dynamics (in this preliminary experimental campaign braces had no specific function, and in the final controlled configuration they would have been connected to the floors and their dynamics would have been dramatically modified), partly because it was judged unlikely that a close tuning might occur between the braces and some structural mode. This kind of model, reasonable until the influence of NSEs was correctly understood, will be taken herein as representative of the incorrect modelling of S-NSEs, in the sense explained in previous sections.

According to this model, stiffness and mass matrices are statically condensed to the six translational and rotational displacement components of the first and second floors' geometrical centres, included in the vector $\eta = \{d_{x1}, d_{y1}, d_{\theta 1}, d_{x2}, d_{x2}, d_{\theta 2}\}^{T}$, under the hypotheses of axial rigidity of Euler-Bernoulli type columns and beams, in-plane rigidity of floor slabs, and lumped mass formulation for columns and beams. Columns are assumed clamped at their base (i.e. no dynamics is attributed to the base level), no connection is explicitly recognized between the floor slabs and the steel beams, and each of the additional concrete blocks is modelled as a translational inertia, entering the system mass matrix with its own mass, static moment and polar inertia. With these assumptions, for each of the three mass configurations, the resulting 6-DOF baseline, or nominal, model (prior to calibration) is obtained through equalling each geometrical and mechanical parameter to its expected (nominal) value. A list of the main nominal parameters assigned to the baseline model is given in Table 2. An axonometric view of the 6-DOF baseline model in the BC configuration is given in Fig. 9, together with a planar schematic view of its six mode-shapes.

4.3 **The experimental modal model**

The experimental modal model is identified on the basis of ambient vibration tests. Three classical output-only methods are used (and compared to enhance robustness) in order to extract frequencies and mode-shapes, respectively working in the time-domain, in the frequency-domain and in the time-frequency domain: NExT/ERA [36], FDD [37] and TFIE [38].

Details of the experimental modal analysis can be found in [39]. Two results in particular deserve mentioning, clearly recognizable in both Fig. 10, which presents the phase difference standard deviations obtained through the TFIE method, and in Table 3, which reports the mean values and the normalized standard deviations of the experimental natural frequencies and mode-shape components. The first, expected result is the progressive reduction of all structural frequencies as a consequence of the deployment of the additional concrete blocks on the floors, together with a slight modification of the mode-shapes (including appearance of torsional components in the NC configuration). The second result is the existence of seven structural modes instead of the expected six ones. Two modes in particular show different frequencies but nearly undistinguishable mode-shapes, very similar to the second flexural mode of the "incorrect" baseline model in the transverse (y) direction, i.e. to mode 4, and consequently denoted as modes 4a and 4b in what follows.

Useful suggestions on how to interpret these findings come from Fig. 11, which reports the auto-spectral densities of the acceleration signals measured in the transverse direction at, respectively, the ground level, the first storey level, the second storey level and the top of one of the lower braces (i.e. those attached to the base level, see again Fig. 8). First of all, Fig. 11 ensures that modes 4a and 4b are true physical modes, and not the effect of identification errors or anomalous narrow-band external input: the two respective peaks, migrating

leftwards as the structural mass increases, are prominent in the spectra corresponding to the two storey levels whilst are nearly absent from the spectrum corresponding to the ground level, in contrast with the small peak around 7.8 Hz, which appears almost identical for all spectra and independent of the mass configuration, and which can be clearly attributed to the input frequency content. Besides, above all, Fig. 11 draws attention to the so far neglected influence of the V-inverted braces, indicating that: (i) an interaction occurs between the spectrum corresponding to the lower brace and the spectra corresponding to the first and second storeys, in that modes 4a and 4b produce high peaks in the brace spectrum, and on its turn the brace causes small but distinct perturbations in the structural spectra; such interaction is even more remarkable in that it regards one of the lower braces (the only instrumented one, unfortunately), attached to the base level and not directly to the in-elevation structure; (ii) the natural frequency of the out-of-phase local mode of the instrumented lower brace is close to modes 4a and 4b, and approximately equal to 9 Hz.

These findings suggest a nice physical interpretation of modes 4a and 4b, based on the concept of modal interaction illustrated in previous sections. Accordingly, these two modes would emerge from the interaction between the MS and the out-of-plane mode of the upper braces (those attached to the first floor, unfortunately not instrumented), accidentally working as a couple of S-NSEs roughly tuned to the fourth mode of the benchmark structure. The total effective resonant mass, approximately including the two gusset plates atop and half the mass of the four HE100A diagonals, is around 140 kg. This value, apparently small if compared with the total mass of the building (about 6600 kg), is indeed large enough, if compared with the modal mass of the fourth mode (approximately 500 kg according to the subsequent model calibration), to justify the observed phenomenon.

4.4 **The augmented FE model (including NSEs)**

The "incorrect" 6-DOF model is inadequate to explain the experimentally identified seven modes. In order for modes 4a and 4b to be fairly reproduced by the model, the latter needs to be augmented so as to account for the two resonant S-NSEs. This is done by incorporating in the original 6-DOF model two identical single-DOF appendages, attached to the first storey and corresponding to the transverse dynamics of the two upper V-inverted braces. The nominal mass of each appendage, denoted as m_s, is assumed equal to a rough estimation of the effective resonant mass of the S-NSE, i.e. 70 kg. The nominal frequency of each appendage, denoted as f_s, is assumed equal to 10 Hz, i.e. to the approximate average of f_{4a} and f_{4b} for the three mass configurations (see again the auto-spectra in Fig. 11).

An axonometric view of the resulting 8-DOF baseline model in the BC configuration is given in Fig. 12, together with a planar schematic view of its eight mode-shapes. Comparing Fig. 12 with Fig. 9, it is clear that including the NSEs into the model does not alter the five modes which are far from the NSEs' frequency but substantially alter mode 4, due to its frequency, 9.65 Hz, being close to the NSEs' frequency, 10 Hz. Instead of the original mode 4, three modes now exist, originated from the interaction of mode 4 with the two NSEs' modes. Of these three modes, the lower and the upper ones, respectively denoted as mode 4a (f_{4a} = 9.10 Hz) and mode 4b (f_{4b} = 10.8 Hz), correspond to the experimentally identified interacting modes introduced in the previous subsection 4.3; looking at their mode-shapes, it is clear that the two additional DOFs (circles in Fig. 12) are in phase with each other, and respectively in phase (mode 4a) and in counter-phase (mode 4b) with the first storey level (grey line) to which they are attached; it is also clearly visible that, as long as the NSEs are not instrumented, mode-shapes 4a and 4b appear practically indistinguishable from each other and from mode 4 of the MS. On the other hand, the intermediate of these three modes, denoted as mode 4ab (f_{4ab} = 10.0 Hz), does not correspond to any of the identified modes; its frequency is exactly the frequency of the two NSEs and its mode-shape has null components at all 6 DOFs of the MS, and equal and opposite components at the 2 DOFs of the NSEs; evidently, since the upper V-inverted braces were not instrumented during testing, this mode is not identifiable from measured data.

4.5 **Model calibration according to Approaches 1 to 3**

The three approaches presented in Section 3 are here applied to the real case study. Since, however, in this case the exact solution is not known in advance, caution must be used to select the proper set of updating parameters. A multi-model updating procedure is adopted in order to enhance robustness, consisting in comparing alternative optimal models obtained using different updating sets [40]. As in Section 3, the solution of the updating problem entails minimization of an objective function which measures the distance between the experimental and the numerical modal models. The objective function, again defined by Eq. (6), now extends to the whole of the three mass configurations (BC, NC, SC), and for each mass configuration includes 6 modes in Approach 1, 5 modes in Approach 2, and 7 modes in Approach 3. According to the multi-model procedure, the overall set of potential updating parameters ("potential set"), normalized to their respective nominal values, is identified first, based on the available *a priori* knowledge and on a sensitivity analysis (Fig. 13). Twelve parameters are thus identified as potential candidates for updating, including mass and polar inertias of the floor

slabs, bending stiffness of columns and beams, mass and frequency of the NSEs when relevant (refer to Table 2 again). Then, in order to avoid ill-conditioning or indeterminateness of the optimization problem, three different plausible subsets of the potential set ("updating sets" or "models") are chosen for each approach, denoted as M_1, M_2 and M_3 for Approaches 1 and 2 (incorrect modelling of NSEs), and as M_{1+}, M_{2+} and M_{3+} for Approach 3 (correct modelling of NSEs), and the minimization problem is separately solved for each model and for each approach.

Results are reported in Tables 4 to 7. As in Section 3, Approach 1 is presented twice, according as either f_{4a} (Approach 1-a) or f_{4b} (Approach 1-b) are chosen for updating. In order to genuinely capture improvements in the model, the multiple solutions are compared in terms not only of their modal fitting capability (f_{ob}) but also of the plausibility of the underlying parametric description. Using, as in Table 1, the RMS error to measure the distance in the parameter domain between different solutions, it results that the distance from the best model (M_{3+}) equals 17.6% for M_3 according to Approach 1a, 72.9% for M3 according to Approach 1b, and only 2.1% for M_3 according to Approach 2.

4.6 Discussion of the results

Looking at the results in Tables 4 to 7 the following considerations can be formulated.

The best model is M_{3+} calibrated using Approach 3. This model is the analogue of the exact model in Section 3 and can be used here as the reference term for evaluating any other solution. This model not only achieves an excellent matching of the experimental modal data, testified by the small value of the objective function (f_{ob3} = 0.659%) and further appreciable by comparing Table 3 above (experimental modal data) with Table 8 below (simulated modal data), but it also possesses clearly sound physical meaning. The stiffness of the lower columns is less than nominal ($\overline{I}_{cx1}$ = 0.607, $\overline{I}_{cy1}$ = 0.769), coherently with the plausible imperfect clamp at their base, and the stiffness of the beams is larger than nominal ($\overline{I}_{bx}$ = 1.305, $\overline{I}_{by}$ = 1.163), coherently with the plausible collaboration of the floor slabs. The mass and frequency of the S-NSEs are coherent with expectations ($\overline{m}_s$ = 1.062, $\overline{f}_s$ = 1.011), proving that estimating the effective resonant mass based on NSEs' geometry and the resonant frequency as the average of frequencies f_{4a} and f_{4b} is an acceptable approximation. If, in order to represent the floor sagging effect, the slab thickness at the i-th level, t_i, is expressed as a 4th order polynomial function of x and y according to:

$$t_i(x,y) = s_i + f_i[1-(2x/L_x)^2][1-(2y/L_y)^2] \tag{7}$$

in which L_x and L_y are the slab dimensions along x and y, s_i is the uniform thickness at the i-th level, and f_i is the mid-span additional deflection at the i-th level, then the masses and polar inertias identified in model M_{3+} exactly lead to s_1 = 7.5 cm, s_2 = 6.7 cm, f_1 = 2.7 cm and f_2 = 4.1 cm (resulting in total mid-span deflections s_1 + f_1 = 10.2 cm and s_1 + f_1 = 10.8 cm), in good agreement with visual inspections. Finally, an interesting confirmation of the plausibility of model M_{3+}, not available at the time when model updating was first performed, came later on, when an accelerometer placed on one of the upper braces revealed an out-of-plane frequency of 10.0 Hz, very close to the best calibrated value of 10.1 Hz.

It deserves noticing that the same Approach 3 gives not so good results for updating sets M_{1+} and M_{2+}, because they both exclude beams' stiffness from calibration. This result confirms the importance of correctly choosing the set of updating parameters, which can be profitably done, for instance, by recurring to multi-model approaches. Nonetheless, no matter which of the three updating sets is chosen, the mass and frequency of the NSEs are identified with very good accuracy and minimum dispersion ($\overline{m}_s$ ranges from 1.025 for M_{1+} to 1.084 for M_{2+}, and $\overline{f}_s$ ranges from 1.011 for M_{3+} to 1.020 for M_{1+}), testifying that Approach 3 can successfully identify NSEs' dynamic behaviour independently of modelling errors and, remarkably, with no need to take measurements on them.

Approach 2 provides satisfactory results too. The best model, once again obtained using the updating set M_3, is very close to the M_{3+} model obtained with the Approach 3, both in terms of the objective function (f_{ob3} = 0.780%) and in terms of the distance in the search domain: the RMS distance from M_{3+} is only 2.1%, and the maximum distance along a single parameter, $\overline{I}_{cx1}$, is only 3.7%. This clearly confirms the validity of Approach 2. The calibrated model is very close to the best possible one, with no need to modify the model structure through including the resonant NSEs, and modal matching (with the obvious exception of modes 4a and 4b) is good in absolute terms. This is a result of great practical importance, which validates Approach 2 as a simplified

way to acceptably perform model calibration in the presence of resonant NSEs without modifying the FE model of the MS.

On the contrary, as already shown for the numerical case-study in Section 3, Approach 1 shows all its limitations, proving the significance of NSEs and the importance of well understanding their role during experimental modal analysis. Not only the objective function significantly increases with respect to Approaches 2 and 3 but also the updated models diverge significantly from model M_{3+}, particularly if mode 4b is used (Approach 1-b), in which case the RMS distance from M_{3+} grows to an unacceptable 72.9%, with errors of 274% along $\overline{I}_{cy1}$ and -66% along $\overline{I}_{by}$. The physical unsoundness of the resulting solution here luckily alerts that something has gone wrong. Unfortunately, this is not always the case.

5. Conclusions

In the present paper, numerical and experimental case studies are analysed to demonstrate the influence of "resonant" non-structural elements of the "in series" type on the dynamics of the main structure and the need to properly account for their presence when performing experimental modal analysis and model calibration.

Main conclusions of this work can be summarized as follows:

1) non-structural (or secondary structural) elements working in series with the main structure may substantially modify the modal behaviour of the overall system if accidentally tuned to (or "resonating" with) some structural mode; in this event, the structural and the non-structural modes merge together until generating new, combined modes, having frequencies scattered around the original structural frequency and mode-shapes which, as far as no measure is taken on the NSE, are fairly indistinguishable from each other and from the original structural mode-shape; remarkably, the model order is augmented with respect to the model of the bare structure;

2) neglecting the significance of resonant NSEs may cause errors in performing experimental modal analysis (because of the wrong expectation of a lesser model order) as well as in constructing the FE baseline model (because of the exclusion of NSEs from the model structure), therefore potentially invalidating the entire process of model calibration (Approach 1);

3) if, on the contrary, the role of NSEs is correctly understood and an effective experimental modal identification is performed accordingly, two alternative calibration strategies can be pursued, based on respectively excluding from the FE model structure (Approach 2) or including into it (Approach 3) the contribution of non-structural appendages.

These findings highlight a peculiar paradigm of dynamic interaction between structural and non-structural components, which appears to have been mostly disregarded by the literature in the field of experimental system identification and yet may have a significant impact on the effectiveness and reliability of model calibration in real world applications. Tested in this paper only on simple, few-degrees-of-freedom structures, such paradigm is expected to hold even in the case of complex models, and to prove of significant practical interest whenever sufficiently massive, either single or multiple, non-structural appendages happen to be close to resonate with one or several structural modes. The exemplification on large-scale and real-case applications is left for future work.

References

[1] Friswell MI, Mottershead JE (1995) Finite Element Model Updating in Structural Dynamics. Kluwer Academic Press, Dordrecht, the Netherlands.

[2] Saitta A, Raphael B, Smith IFC (2005) Data mining techniques for improving the reliability of system identification. Adv Eng Inform 19:289-298.

[3] Eamon CD, Nowak AS (2004) Effect of secondary elements on bridge structural system reliability considering moment capacity. Struct Saf 2004 26:29-47.

[4] Marefat M-S, Ghahremani-Gargary E, Ataei S (2004) Load test of a plain concrete arch railway bridge of 20-m span. Constr Build Mater 2004 18:661-667.

[5] Mastrogiuseppe S, Rogers CA, Tremblay R, Nedisan CD (2008) Influence of nonstructural components on roof diaphragm stiffness and fundamental periods of single-storey steel buildings. J Constr Steel Res 2008 64:214-227.

[6] Fardis MN (1997) Experimental and numerical investigations on the seismic response of RC infilled frames and recommendations for code provisions. Report ECOEST-PREC8 no. 6. Prenormative research in support of Eurocode 8.

[7] Kim JY, Yu E, Kim DY, Kim S-D (2009) Calibration of analytical models to assess wind-induced acceleration responses of tall buildings in serviceability level. Eng Struct 31:2086-2096.

[8] Goulet J-A, Kripakaran P, Smith IFC (2009) Estimation of modelling errors in structural system identification. Proceedings of the 4th Int. Conf. Struct. Health Monitoring of Intelligent Infrastructure, Zurich.

[9] Turer A, Shahrooz BM (2011) Load rating of concrete-deck-on-steel-stringer bridges using field-calibrated 2D-grid models. Eng Struct 33:1267-1276.
[10] Brownjohn JMW, Dumanoglu AA, Taylor CA (1994) Dynamic investigation of a suspension footbridge. Eng Struct 1994 16:395-406.
[11] Zivanovic A, Pavic A, Reynolds P (2006) Modal testing and FE model tuning of a lively footbridge structure. Eng Struct 28:857-868.
[12] Schubert S, Gsell D, Steiger R, Feltrin G (2010) Influence of asphalt pavement on damping ratio and resonance frequencies of timber bridges. Eng Struct 2010 32:3122-3129.
[13] Su RKL, Chandler AM, Sheikh MN, Lam NTK (2005) Influence of non-structural components on lateral stiffness of tall buildings. Struct Des Tall Special Build 14(2):143-164.
[14] Torkamani MAM, Armadi AK (1998) Stiffness identification of a tall building during construction period using ambient tests. Earthq Eng Struct Dyn 16(8):1177-1188.
[15] Boroschek RL, Baesler H, Vega C (2011) Experimental evaluation of the dynamic properties of a wharf structure. Eng Struct 33:344-356.
[16] Jones CA, Reynolds P, Pavic A (2011) Vibration serviceability of stadia structures subjected to dynamic crowd loads: A literature review. J Sound Vib 330:1531-1566.
[17] Chen Y, Soong TT (1988) State-of-the-Art Review: Seismic Response of Secondary Systems. Eng Struct 10(4):218-228.
[18] Villaverde R (2004) Seismic Analysis and Design of Nonstructural Elements. In: Bozorgnia and Bertero editors. Earthquake Engineering: From Engineering Seismology to Performance-Based Engineering. Boca Raton, USA: CRC Press.
[19] Soong TT (1990) Seismic performance of nonstructural elements during the Loma Prieta earthquake. Report NIST SP 796, 22nd Joint Meeting U.S.-Japan Cooperative Program in Natural Resources Panel on Wind and Seismic Effects, Natl. Inst. of Standards and Technology, Gaithersburg, Maryland, 331-336.
[20] Whitney DJ, Dickerson A, Lindell MK (2001) Nonstructural seismic preparedness of Southern California hospitals. Earthq Spectra 17(1):153-171.
[21] Chaudhuri SR, Hutchinson TC (2004) Distribution of peak horizontal acceleration for estimating nonstructural element vulnerability. Proceedings of the 13th World Conf. on Earth. Eng., Vancouver, Canada, paper 1721.
[22] Lam NTK, Griffith M, Wilson J, Doherty K (2003) Time-history analysis of URM walls in out-of-plane flexure. Eng Struct 25:743-754.
[23] Muscolino G (1990) Dynamic response of multiply connected primary-secondary systems. Earthq Eng Struct Dyn 19:205-216.
[24] Eurocode 8 (2004) Design for structures for earthquakes resistance - part 1: General rules, seismic actions and rules for buildings. EN 1998-1.
[25] Singh MP, Moreschi LM, Suárez LE, Matheu EE (2006) Seismic design forces. I: rigid nonstructural components. J Struct Eng 132(10):1524-1532.
[26] Gupta AK (1984) Seismic response of multiply connected MDOF primary and MDOF secondary systems. Nucl Eng Des 81(3):385-394.
[27] Igusa T, Der Kiureghian A (1985) Generation of floor response spectra including oscillator-structure interaction. Earthq Eng Struct Dyn 13:661-676.
[28] Burdisso RA, Singh MP (1987) Seismic analysis of multiply supported secondary systems with dynamic interaction effects. Earthq Eng Struct Dyn 15:1005-1022.
[29] Muscolino G, Palmeri A (2007) An earthquake response spectrum for linear light secondary substructures. ISET J Earthquake Tech 482(44):193-211.
[30] Warburton GB, Ayorinde EO (1980) Optimum absorber parameters for simple systems. Earthq Eng Struct Dyn 8:197-217.
[31] Villaverde R, Koyama LA (1993) Damped resonant appendages to increase inherent damping in buildings. Earthq Eng Struct Dyn 22:491-507.
[32] Abé M, Igusa T (1995) Tuned mass dampers for structures with closely spaced natural frequencies. Earthq Eng Struct Dyn 24:247-261.
[33] Matta E, De Stefano A, Spencer Jr BF (2009) A new passive rolling-pendulum vibration absorber using a non-axial-symmetrical guide to achieve bidirectional tuning. Earthq Eng Struct Dyn 38:1729-1750.
[34] Matta E (2013), Effectiveness of tuned mass dampers against ground motion pulses. J Struct Eng (ASCE) 139(2): 188-198.
[35] Nalitolela NG, Penny JET, Friswell MI (1992) A mass or stiffness addition technique for structural parameter updating. Int J of Analyt and Exp Modal Analysis 7(3):157-168.

[36] Juang JN, Pappa RS (1984) An eigensystem realisation algorithm (ERA) for modal parameter identification and modal reduction. Proceedings of NASA/JPL Workshop on Identification and Control of Flexible Space Structures.
[37] Brincker R, Zhang L, Andersen P (2001) Modal identification of output-only systems using frequency domain decomposition. Smart Mater Struct 10:441-445.
[38] Bonato P, Ceravolo R, De Stefano A, Molinari F (2001) Use of cross time–frequency estimators for the structural identification in non-stationary conditions and under unknown excitation. J Sound Vib 237:775-791.
[39] Antonacci E, De Stefano A, Gattulli V, Lepidi M, Matta E (2012) Comparative study of vibration-based parametric identification techniques for a three-dimensional frame structure. Struct Control Hlth 19(5):579-608.
[40] Matta E, De Stefano A (2012) Robust finite element model updating of a large-scale benchmark building structure. Struct Eng Mech 43(3):371-394.

List of captions

Fig. 1 NSEs on a single-DOF structure: (a) MS; (b) MS with a P-NSE; (c) MS with an S-NSE

Fig. 2 NSEs on a shear-type 3-storey building structure: (a) MS; (b) MS with a P-NSE (in-plane infill); (c) MS with an S-NSE (pendulous mass); (d) MS with an S-NSE (out-of-plane infill)

Fig. 3 Input-output transfer functions for a shear-type 3-storey building with different arrangements of NSEs (Cases (a) to (f) in the respective six sub-figures), either correctly modelled (thick lines) or incorrectly modelled (contours of grey areas)

Fig. 4 Natural frequencies and mode-shapes for Cases (a) to (f): correct modelling (marks) vs. incorrect modelling (continuous lines)

Fig. 5 3rd storey acceleration under real seismic records for, respectively, correctly and incorrectly modelled NSEs: (a) Case (e) – Record # 0143 TAB-LN; Case (f) – Record # 1529 TCU102-N

Fig. 6 Response ratio under the whole set of 338 records from the PEER-NGA Strong Motion Database: (a) Cases (e) and (f); (b) and (c) Case (f^*) for different values of the frequency ratio r

Fig. 7 Case (f^*) – Mean, 5% and 95% percentile response ratios as a function of the frequency ratio, under the whole set of 338 records, for different values of the mass ratio μ

Fig. 8 The test structure: (a) overall view; (b) location of accelerometers and additional blocks

Fig. 9 The 6-DOF, "incorrect" FE baseline model in the BC configuration: (left) axonometric view; (right) planar view of the 6 mode-shapes (dotted line: base level; grey line: first level; black line: second level)

Fig. 10 Phase difference standard deviations for the identification of modal frequencies using TFIE method, referring to, respectively, the BC (left), NC (centre) and SC (right) configurations

Fig. 11 Auto-spectral densities (at the ground level, the 1st storey level, the 2nd storey level and the top of one of the lower braces) in the along-y direction for, respectively, the BC (left), NC (centre) and SC (right) configurations

Fig. 12 The 8-DOF, "correct" FE baseline model in the BC configuration: (left) axonometric view; (right) planar view of the 8 mode-shapes (dotted line: base level; grey line: first level; black line: second level; circles: NSEs)

Fig. 13 Scheme of the "correct" FE model illustrating the 12 potential updating parameters

List of figures

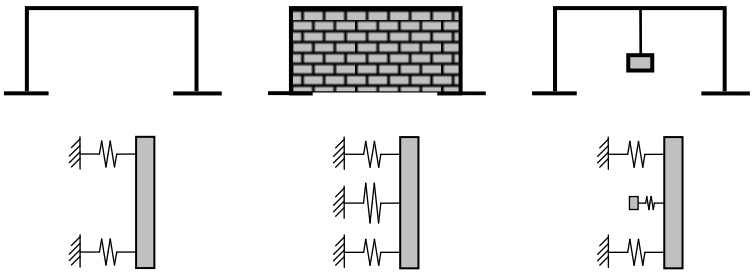


Fig. 1 NSEs on a single-DOF structure: (a) MS alone; (b) MS with a P-NSE; (c) MS with an S-NSE

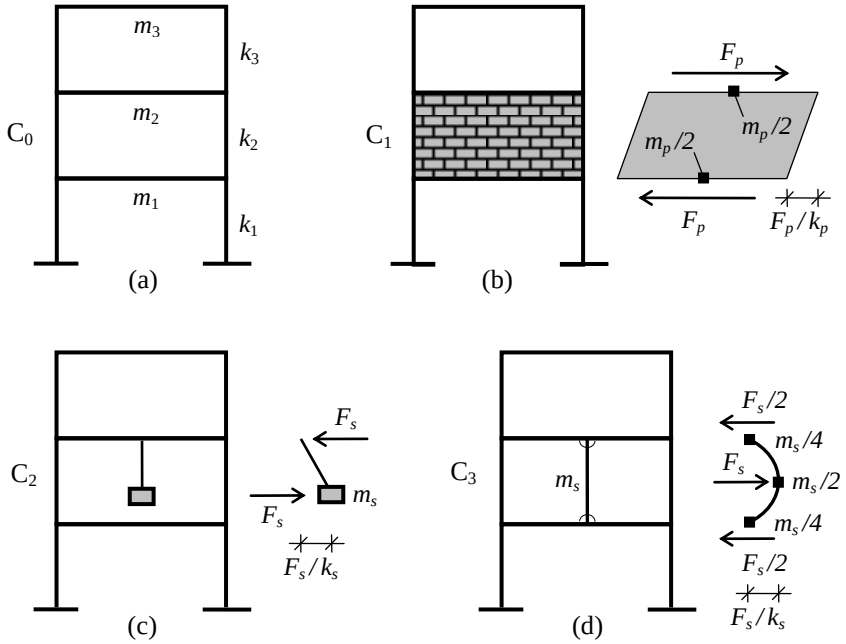


Fig. 2 NSEs on a shear-type 3-storey building structure: (a) MS; (b) MS with a P-NSE (in-plane infill); (c) MS with an S-NSE (pendulous mass); (d) MS with an S-NSE (out-of-plane infill)

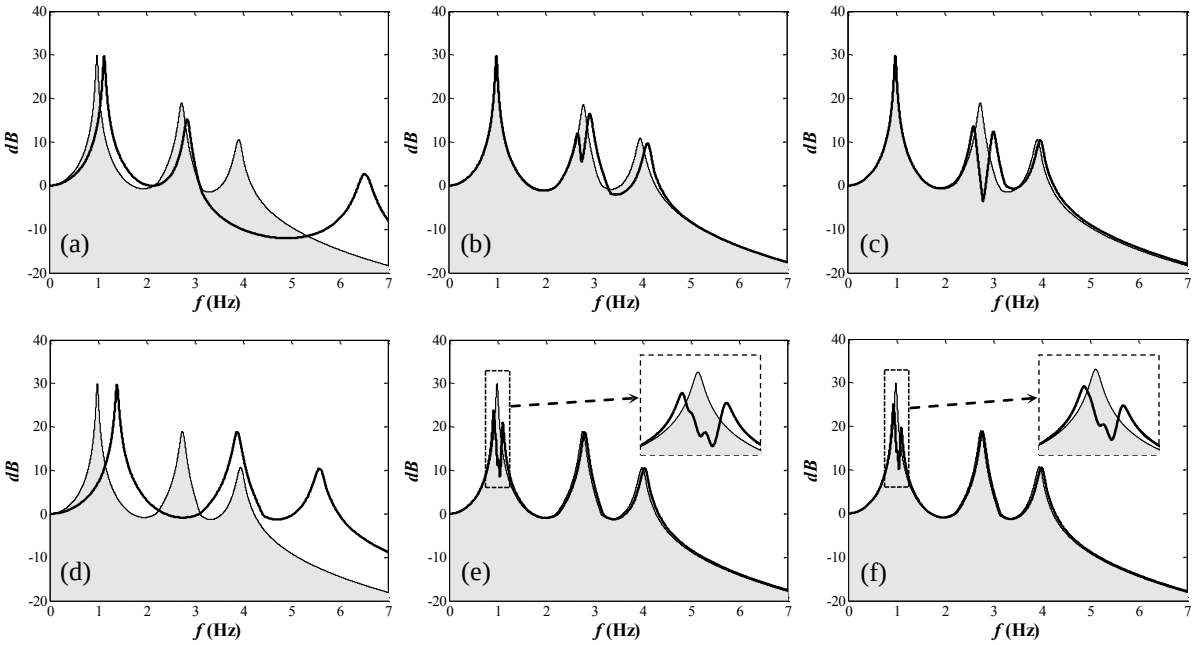


Fig. 3 Input-output transfer functions for a shear-type 3-storey building with different arrangements of NSEs (Cases (a) to (f) in the respective six sub-figures), either correctly modelled (thick lines) or incorrectly modelled (contours of grey areas)

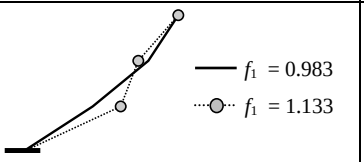
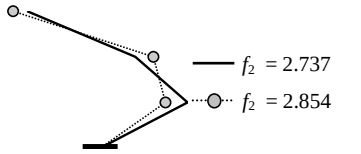
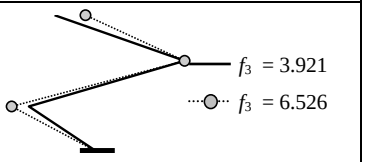
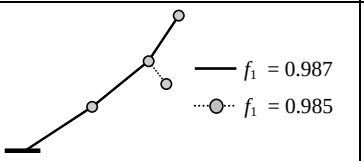
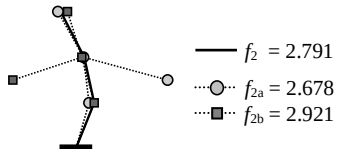
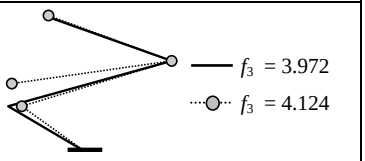
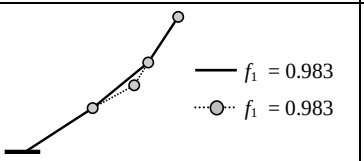
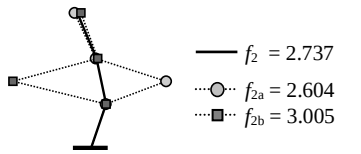
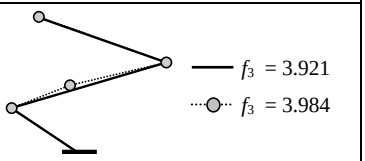
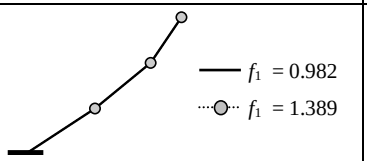
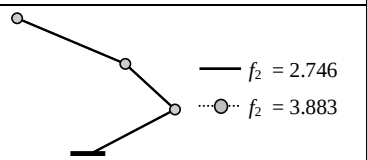
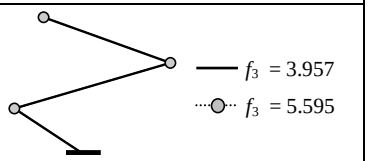
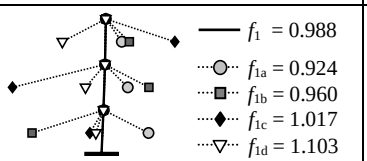
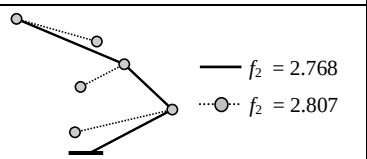
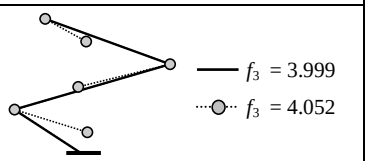
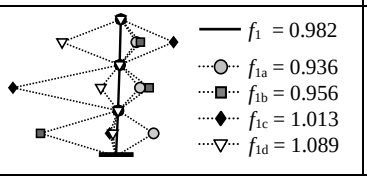
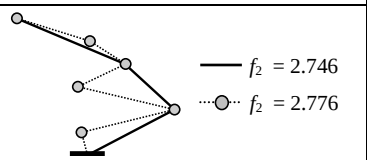
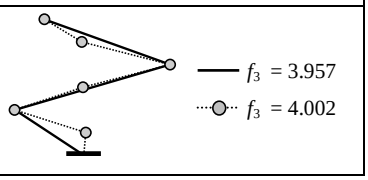
Case	1st mode	2nd mode	3rd mode
(a)			
(b)			
(c)			
(d)			
(e)			
(f)			

Fig. 4 Natural frequencies and mode-shapes for Cases (a) to (f): correct modelling (marks) vs. incorrect modelling (continuous lines)

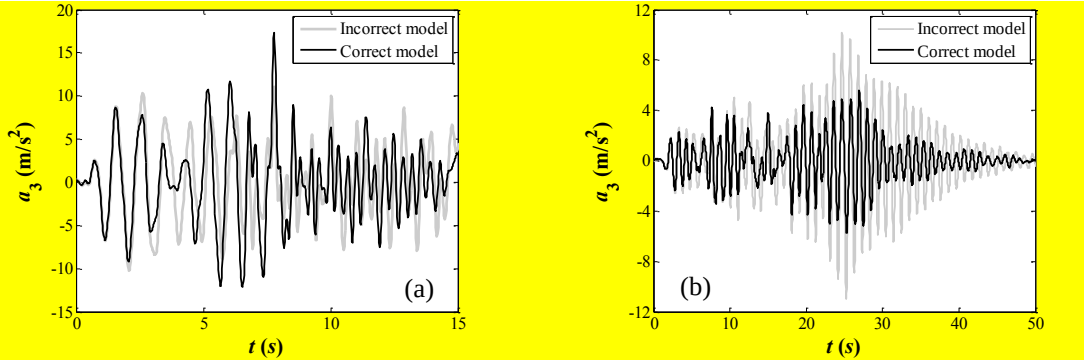


Fig. 5 3rd storey acceleration under real seismic records for, respectively, correctly and incorrectly modelled NSEs: (a) Case (e) – Record # 0143 TAB-LN; Case (f) – Record # 1529 TCU102-N

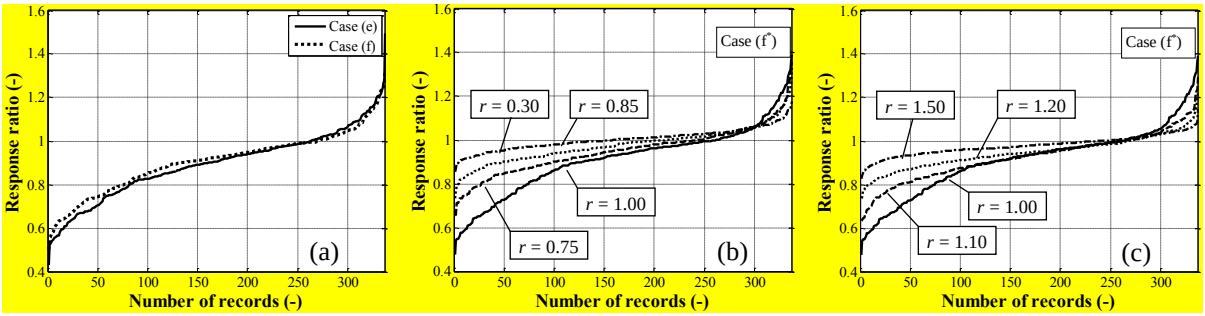


Fig. 6 Response ratio under the whole set of 338 records from the PEER-NGA Strong Motion Database: (a) Cases (e) and (f); (b) and (c) Case (f^*) for different values of the frequency ratio *r*

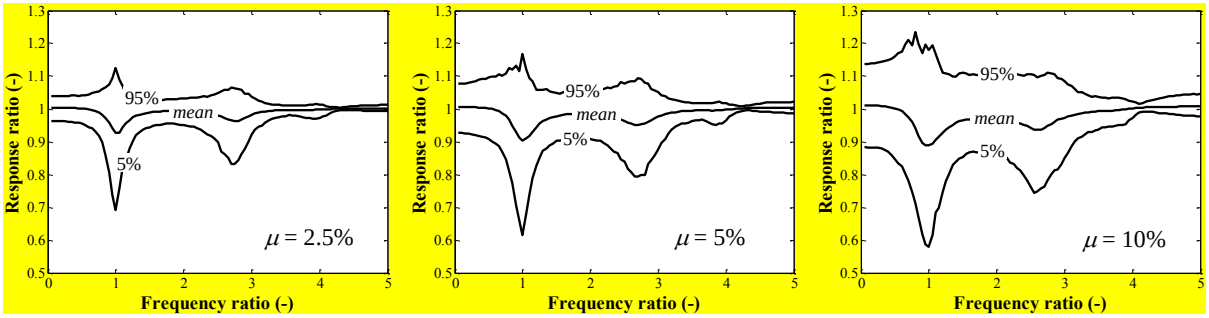
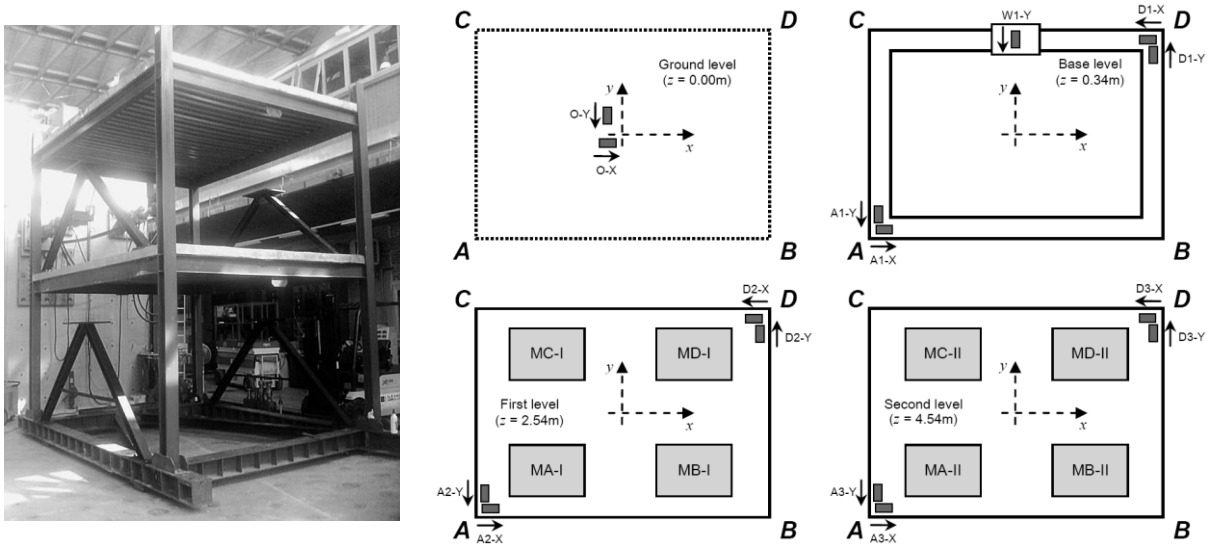


Fig. 7 Case (f^*) – Mean, 5% and 95% percentile response ratios as a function of the frequency ratio, under the whole set of 338 records, for different values of the mass ratio μ



(a) (b)

Fig. 8 The test structure: (a) overall view; (b) location of accelerometers and additional blocks

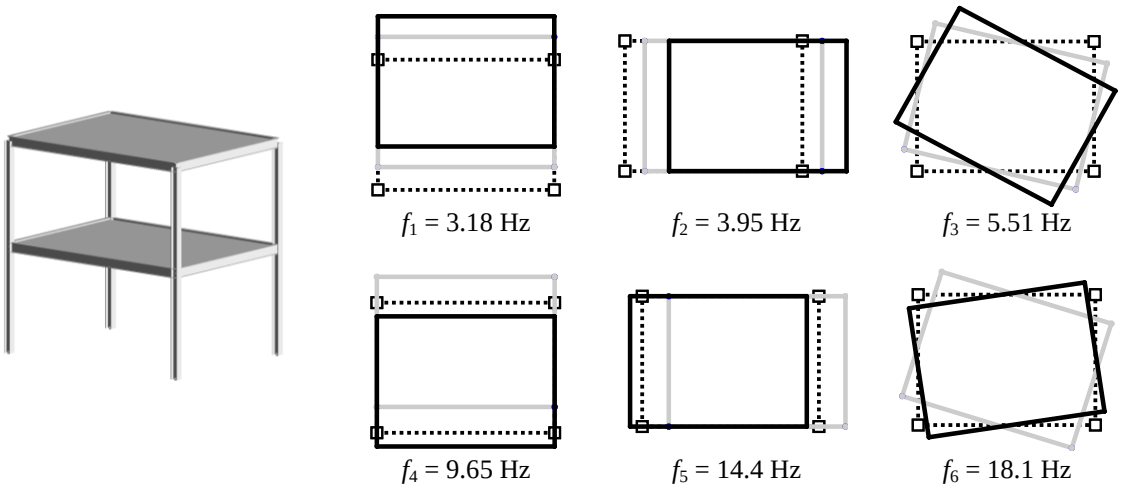


Fig. 9 The 6-DOF, “incorrect” FE baseline model in the BC configuration: (left) axonometric view; (right) planar view of the 6 mode-shapes (dotted line: base level; grey line: first level; black line: second level)

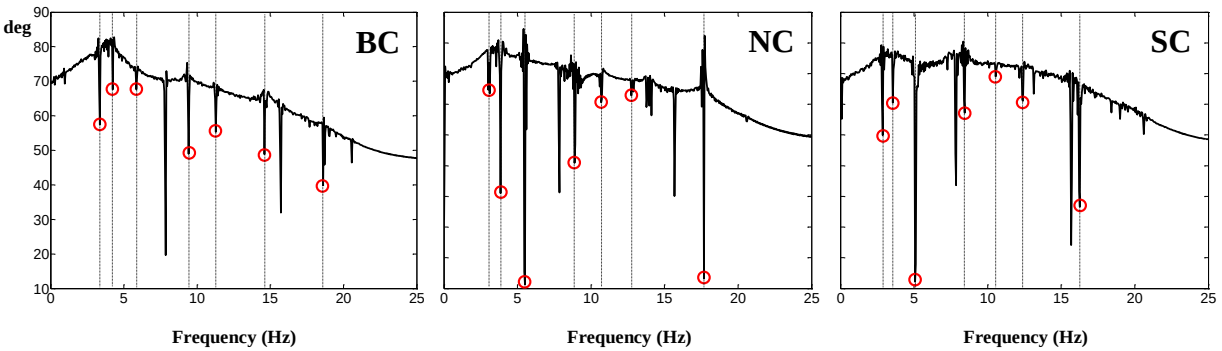


Fig. 10 Phase difference standard deviations for the identification of modal frequencies using TFIE method, referring to, respectively, the BC (left), NC (centre) and SC (right) configurations

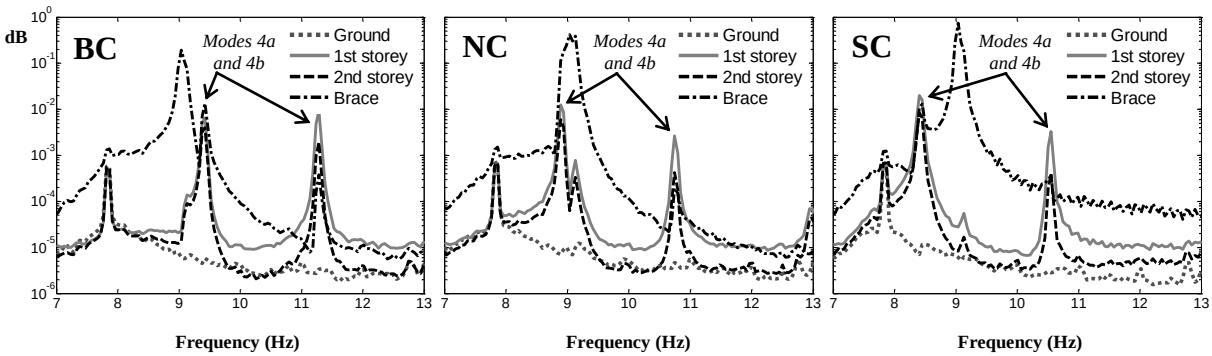


Fig. 11 Auto-spectral densities (at the ground level, the 1st storey level, the 2nd storey level and the top of one of the lower braces) in the along-y direction for, respectively, the BC (left), NC (centre) and SC (right) configurations

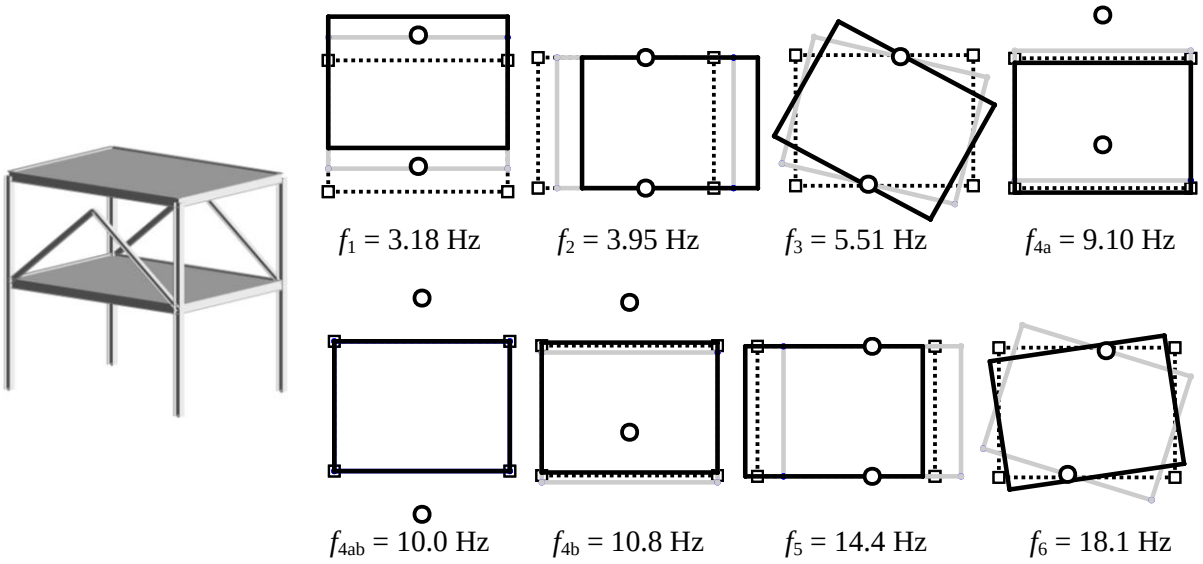


Fig. 12 The 8-DOF, "correct" FE baseline model in the BC configuration: (left) axonometric view; (right) planar view of the 8 mode-shapes (dotted line: base level; grey line: first level; black line: second level; circles: NSEs)

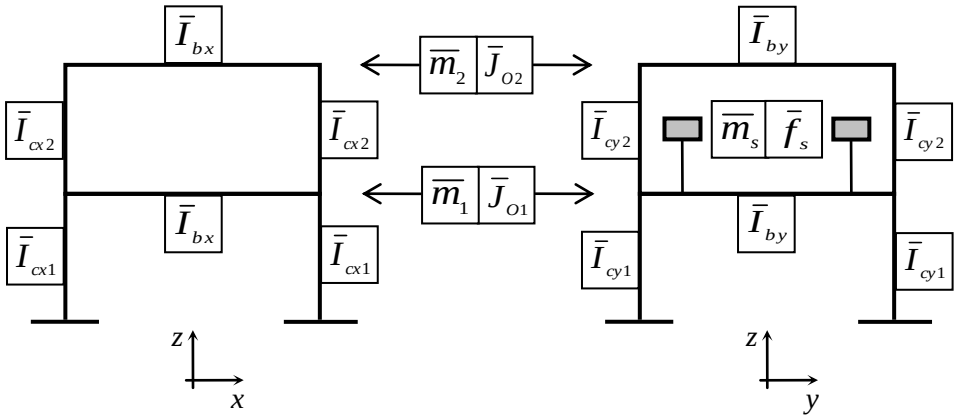


Fig. 13 Scheme of the "correct" FE model illustrating the 12 potential updating parameters

List of tables

Table 1 Model calibration according to Approaches 1, 2 and 3.

Approach	$\overline{k}_1$	$\overline{k}_2$	$\overline{k}_3$	$\overline{k}_s$	d (%)
1-a	0.948	1.159	0.850	n.a.	13.0
1-b	1.350	0.685	1.343	n.a.	33.6
2	0.985	1.045	1.004	n.a.	2.7
3	1.000	1.000	1.000	1.000	0.0

Table 2 Nominal parameters of the baseline FE model.

Symbol	Description	Value	Unit
l_x	Distance between columns along x	4.00	m
l_y	Distance between columns along y	3.00	m
h	Inter-storey height	2.00	m
E	Steel Young's modulus	206	GPa
ρ_s	Steel mass density	7850	kg/m^3
ρ_c	Composite slab mass density	2500	kg/m^3
m_i	Slab mass at the i-th level (i = 1, 2)	3539	kg
J_{oi}	Slab polar inertia (i = 1, 2)	7702	kg·m^2
I_{cxi}	Columns bending inertia along x (i = 1, 2)	$1.509 \cdot 10^{-5}$	m^4
I_{cyi}	Columns bending inertia along y (i = 1, 2)	$0.550 \cdot 10^{-5}$	m^4
I_{bxi}	x-oriented beams bending inertia (i = 1, 2)	$1.317 \cdot 10^{-5}$	m^4
I_{byi}	y-oriented beams bending inertia (i = 1, 2)	$1.317 \cdot 10^{-5}$	m^4

Table 3 Experimental modal properties – Mean values (‰ standard deviation in brackets).

Conf.	Mode	f_{ei} (Hz)	ϕ_{ei1}	ϕ_{ei2}	ϕ_{ei3}	ϕ_{ei4}	ϕ_{ei5}	ϕ_{ei6}
	1	3.37 (.3)	-.009	.507 (6)	.001	-.005	.862 (2)	.004
	2	4.23 (.6)	.445 (2)	-.004	-.002	.895 (0)	.006	.000
	3	5.89 (.2)	.057	.053	.478 (84)	.054	-.011	.873 (7)
BC	4a	9.39 (.6)	.026	.777 (27)	.006	-.038	-.627 (31)	-.029
	4b	11.3 (.2)	-.031	.913 (10)	.006	-.020	-.405 (69)	-.010
	5	14.6 (.1)	.876 (5)	.000	.004	-.483 (15)	.005	-.005
	6	18.7 (.1)	-.006	-.071	.828 (30)	-.006	.011	-.555 (41)
	1	3.08 (.5)	-.004	.510 (9)	.005	-.007	.860 (3)	.004
	2	3.85 (.7)	.448 (3)	-.004	.027	.892 (1)	.002	.049
	3	5.51 (.6)	-.120	.010	.470 (12)	-.276	-.032	.829 (8)
NC	4a	8.90 (.4)	.012	.825 (5)	.000	.004	-.565 (10)	-.017
	4b	10.7 (.1)	.020	.927 (7)	.011	.022	-.372 (23)	-.020
	5	12.9 (.3)	.868 (0)	-.081	.084	-.475 (58)	.027	-.082
	6	17.6 (.0)	-.247	-.011	.806 (8)	.196	.021	-.501 (10)
	1	2.85 (.5)	-.004	.505 (6)	-.001	-.004	.863 (3)	.005
	2	3.57 (.6)	.447 (4)	-.002	-.001	.894 (1)	.007	-.001
	3	5.11 (.1)	-.005	.012	.495 (39)	.019	-.015	.868 (18)
SC	4a	8.43 (.4)	.003	.840 (5)	.002	-.004	-.542 (9)	-.012
	4b	10.5 (.1)	-.001	.944 (8)	.001	-.006	-.329 (65)	-.011
	5	12.4 (.2)	.880 (7)	-.005	.002	-.474 (24)	.002	-.004
	6	16.2 (.1)	-.016	-.062	.851 (12)	.022	.008	-.520 (24)

Table 4 Approach 1-a.

Model	$\bar{I}_{cx1}$	$\bar{I}_{cy1}$	$\bar{I}_{cx2}$	$\bar{I}_{cy2}$	$\bar{I}_{bx}$	$\bar{I}_{by}$	$\bar{m}_1$	$\bar{m}_2$	$\bar{J}_{O1}$	$\bar{J}_{O2}$	$\bar{m}_s$	$\bar{f}_s$	f_{ob1a} (%)
M_1	.952	.928	1	1	1	1	1.045	.794	.946	.793	n.a.	n.a.	1.26
M_2	.881	.913	1.099	0.989	1	1	1.041	.774	.944	.766	n.a.	n.a.	1.23
M_3	.952	.857	1	1	.984	1.137	1.035	.789	.928	.804	n.a.	n.a.	1.24

Table 5 Approach 1-b.

Model	$\bar{I}_{cx1}$	$\bar{I}_{cy1}$	$\bar{I}_{cx2}$	$\bar{I}_{cy2}$	$\bar{I}_{bx}$	$\bar{I}_{by}$	$\bar{m}_1$	$\bar{m}_2$	$\bar{J}_{O1}$	$\bar{J}_{O2}$	$\bar{m}_s$	$\bar{f}_s$	f_{ob1b} (%)
M_1	0.451	0.658	1	1	1	1	.528	.628	0.666	.515	n.a.	n.a.	4.89
M_2	1.172	0.825	.732	2.510	1	1	.973	.870	1.226	.933	n.a.	n.a.	2.31
M_3	0.820	2.873	1	1	1.155	.395	.960	.837	1.221	.812	n.a.	n.a.	2.10

Table 6 Approach 2.

Model	$\bar{I}_{cx1}$	$\bar{I}_{cy1}$	$\bar{I}_{cx2}$	$\bar{I}_{cy2}$	$\bar{I}_{bx}$	$\bar{I}_{by}$	$\bar{m}_1$	$\bar{m}_2$	$\bar{J}_{O1}$	$\bar{J}_{O2}$	$\bar{m}_s$	$\bar{f}_s$	f_{ob2} (%)
M_1	.756	.792	1	1	1	1	.887	.716	.830	.694	n.a.	n.a.	.856
M_2	.782	.778	.915	1.073	1	1	.862	.726	.834	.707	n.a.	n.a.	.843
M_3	.629	.755	1	1	1.254	1.192	.816	.777	.790	.740	n.a.	n.a.	.780

Table 7 Approach 3.

Model	$\bar{I}_{cx1}$	$\bar{I}_{cy1}$	$\bar{I}_{cx2}$	$\bar{I}_{cy2}$	$\bar{I}_{bx}$	$\bar{I}_{by}$	$\bar{m}_1$	$\bar{m}_2$	$\bar{J}_{O1}$	$\bar{J}_{O2}$	$\bar{m}_s$	$\bar{f}_s$	f_{ob3} (%)
M_{1+}	.711	.772	1	1	1	1	.839	.705	.807	.673	1.025	1.020	.839
M_{2+}	.806	.788	.836	1.028	1	1	.830	.735	.800	.716	1.084	1.013	.739
M_{3+}	.607	.769	1	1	1.305	1.163	.803	.785	.785	.742	1.062	1.011	.659

Table 8 Simulated modal properties of the best calibrated model M_{3+}.

Conf.	Mode	f_i (Hz)	ϕ_{i1}	ϕ_{i2}	ϕ_{i3}	ϕ_{i4}	ϕ_{i5}	ϕ_{i6}
BC	1	3.38	.000	.506	.000	.000	.863	.000
	2	4.24	.468	.000	.000	.884	.000	.000
	3	5.87	.000	.000	.487	.000	.000	.873
	4a	9.38	.000	.780	.000	.000	-.626	.000
	4a-b	10.1	.000	.000	.000	.000	.000	.000
	4b	11.3	.000	.909	.000	.000	-.417	.000
	5	14.5	.876	.000	.000	-.483	.000	.000
	6	18.6	.000	.000	.853	.000	.000	-.521
NC	1	3.08	.000	.505	.000	.000	.863	.000
	2	3.84	.467	.000	.032	.882	.000	.058
	3	5.52	-.141	.000	.464	-.268	.000	.832
	4a	8.92	.000	.822	.000	.000	-.570	.000
	4a-b	10.1	.000	.000	.000	.000	.000	.000
	4b	10.8	.000	.928	.000	.000	-.373	.000
	5	13.2	.874	.000	.074	-.478	.000	-.046
	6	17.6	-.299	.000	.803	.174	.000	-.485
SC	1	2.84	.000	.505	.000	.000	.863	.000
	2	3.57	.468	.000	.000	.884	.000	.000
	3	5.12	.000	.000	.487	.000	.000	.874
	4a	8.42	.000	.838	.000	.000	-.545	.000
	4a-b	10.1	.000	.000	.000	.000	.000	.000
	4b	10.5	.000	.945	.000	.000	-.326	.000
	5	12.3	.878	.000	.000	-.478	.000	.000
	6	16.3	.000	.000	.859	.000	.000	-.513